AIAA-90-0306
Embedded Function Methods for Supersonic Turbulent Boundary Layers

J. He, J. Y. Kazakia and J. D. A. Walker
Lehigh University
Bethlehem, PA

28th Aerospace Sciences Meeting
January 8-11, 1990/Reno, Nevada

EMBEDDED FUNCTION METHODS FOR SUPERSONIC TURBULENT BOUNDARY LAYERS†

J. He*, J. Y. Kazakia** and J. D. A. Walker***
Department of Mechanical Engineering and Mechanics
Lehigh University, Bethlehem, PA 18015

Abstract

The development of embedded functions to represent the mean velocity and total enthalpy distributions in the wall layer of a supersonic turbulent boundary layer is considered. The asymptotic scaling laws (in the limit of large Reynolds number) for high speed compressible flows are obtained to facilitate eventual implementation of the embedded functions in a general prediction method. A self-consistent asymptotic structure is derived, as well as a compressible law of the wall in which the velocity and total enthalpy are logarithmic within the overlap zone, but in the Howarth-Dorodnitsyn variable. Simple outer region turbulence models are proposed (some of which are modifications of existing incompressible models) to reflect the effects of compressibility. As a test of the methodology and the new turbulence models, a set of self-similar outer region profiles is obtained for constant pressure flow; these are then coupled with embedded functions in the wall layer. The composite profiles thus obtained are compared directly with experimental data and good agreement is obtained for flows with Mach numbers up to 10.

Principal Nomenclature

B_o,B_i	Thermal analogs of C_o, C_i
C_o, C_i	Outer, inner logarithmic law constants for velocity
C_p^*	Specific heat at constant pressure
c_p	Constant in Baldwin-Lomax model
F	u/U_e
F_1	Outer scaled stream function deficit
H	Total enthalpy
I	H/H_e
k	Thermal conductivity
K,K_h	Eddy viscosity and conductivity constants (0.0168, 0.0245)
M_e	Mach number at the edge of boundary layer
n	Normal coordinate
p	Pressure
Pr	Prandtl number
q	Total heat flux
q_*	Normalized heat flux at the wall (Equation (4.12))
r	Radius of revolution of axisymmetric body
Re	Reference Reynolds number
Re_{δ_*}	Reynolds number based on displacement thickness (Equation (7.1))
s	Streamwise coordinate
S	Constant in Sutherland formula
T	Temperature
u	Streamwise velocity
U_e	Streamwise velocity at the mainstream
u_τ	Friction velocity
u_*	u_τ/U_e
U^+	Wall-layer scaled streamwise velocity
v	Normal velocity
V	Outer normal velocity (transformed)
Y	Howarth-Dorodnitsyn variable
Y^+	Y/Δ_i, scaled inner normal variable
α	Parameter defined by Equation (2.24)
γ	Ratio of specific heats
γ_0	Euler's constant (= 0.577215....)
δ^*	Incompressible displacement thickness
Δ_o,Δ_i	Outer, inner length scales
ϵ,$\tilde{\epsilon}$,ϵ_H,$\tilde{\epsilon}_H$	Eddy viscosities and eddy conductivities (Equations (5.8), (5.13))
η	rY/Δ_o
Θ , θ^+	Outer, inner total enthalpy defect
κ, κ_θ	von Karman constant and its thermal analog
μ	Absolute viscosity
ξ	Streamwise Mangler coordinate
ρ	Density
σ	Turbulent shear stress
τ	Total shear stress
ϕ	Turbulent heat flux
ψ	Streamfunction
Subscript e	Boundary-layer edge
Subscript w	Wall
Superscript *	Dimensional quantities

* Graduate Research Assistant
** Professor
*** Professor, Member AIAA
† Work supported by NASA Langley Research Center under grant NAG-1-832

1. Introduction

Computation of high speed compressible turbulent flows near solid walls is hampered by several practical difficulties, some of which are associated with the turbulence models (or lack thereof) while others are primarily computational in nature (for a given turbulence model). First consider the turbulence models which are currently in use for the momentum equation. For simplicity, the discussion will relate primarily to algebraic turbulence models. Note, however, that some of the most critical issues are associated with the nature and functional form of the velocity and temperature profiles in the overlap zone near the wall, where both profiles exhibit a logarithmic dependence on normal distance from the wall; consequently, these same aspects are also critical when higher-order closure schemes are used. Examples of algebraic models that are currently in common use include the Cebeci-Smith[1] model and the Baldwin-Lomax[2] model. The essence of these

models is a simple ramp function for eddy viscosity (see also Mellor and Gibson[3]) which behaves linearly in distance from the wall in the near-wall region and then abruptly changes to a constant (at a fixed streamwise location) whose value depends on the local flow conditions; so-called "intermittancy" factors can also be introduced[1,2] as an option, in order to reduce the eddy viscosity to zero far from the wall. The eddy viscosity formula is typically modified[1,2] to a mixing length formulation in the wall-layer region (between the wall and the overlap zone); the mixing length is linear in the overlap zone, but is reduced toward the wall through multiplication by a Van Driest damping factor[1]. Because of the rapid variation of the damping factor and of the velocity profile, relatively large numbers of mesh points are required in the wall layer to ensure reasonable accuracy in any computational algorithm which seeks to compute the velocity profile all the way to the wall.

It is well known that algebraic turbulence models produce good predictions for attached turbulent flows[1,4] at low to moderate subsonic speeds, where a wealth of reliable experimental data is available to validate the computed results. It has been common practice to then extrapolate the use of such models[1], almost without modification, to the calculation of supersonic turbulent boundary layers[1,5-7]. In the absence of turbulence models which adequately reflect the influence of compressibility, this approach gives plausible predictions for the present, but for the longer term needs to be critically assessed. The use of conventional algebraic models in the supersonic regime (that have been tuned for low speed turbulent boundary-layer flows) implicitly assumes that the "law of the wall" for compressible flow takes a similar form to the incompressible version (see, for example, References 8 and 9). However, the "law of the wall" for compressible flow has been controversial[1,4], and at present the precise functional form cannot be considered well established. There have been a number of attempts in the past to develop a compressible law of the wall[4,10,11], including the effective velocity approach of Van Driest[12] which is described in References 1 and 4. The latter form is developed from a mixing length turbulence model and ultimately yields an incompressible form of the law of the wall but in terms of an "effective velocity"; the latter quantity must be obtained from the actual velocity through a transformation involving an inverse sine function. Maise and McDonald[1,13] found that the effective velocity approach gave good comparisons with measured velocity data in a compressible adiabatic boundary layer, but the agreement was much less impressive in flows with heat transfer. Consequently, the Van Driest method[12] can be viewed as an interesting representation of velocity in the overlap zone, which can be used with confidence only over a limited range of conditions. It is therefore apparent that there is no clear consensus on the form of the logarithmic law in compressible flow (at least to the level of confidence which is associated with the incompressible "law of the wall"). In the present study, a compressible law of the wall is described in which the mean velocity is logarithmic, but in the Howarth-Dorodnitsyn variable[14] (rather than the physical normal distance from the wall).

While the situation regarding the velocity profile is somewhat murky, matters are far worse relative to the temperature distribution, where established theoretical results are scarce. For low speed subsonic flows, the static temperature distribution clearly displays a logarithmic behavior in the overlap zone, and this is readily confirmed by a wide variety of experimental data[14]. However, the value of the slope of the temperature profile in the overlap zone is not universally agreed upon; indeed, unlike the velocity profile, the slope of the temperature profile appears to vary with pressure gradient and local flow conditions[14,15]. In the supersonic range, the total enthalpy plays a similar role to the static temperature at low speeds; however, direct measurements of temperature across the entire boundary layer, and in particular in the overlap zone, are very rare. Consequently, it is difficult to confirm whether a logarithmic region exists for the total enthalpy profile and under what conditions, or to determine the slope with any degree of certainty from existing data. At low speeds, the turbulent heat flux terms in the energy equation are usually modeled by assuming that the eddy conductivity can be related to the eddy viscosity through a turbulent Prandtl number; however, this concept proves to be successful only when semi-empirical relations are introduced so that the turbulent Prandtl number varies with distance across the boundary layer. This, of course, is unsatisfactory and brings into question whether the notion of a turbulent Prandtl number is useful in modeling heat transfer in a boundary layer. For high speed compressible flow, similar modeling concepts are often employed[1,4], as well as various versions of the Crocco relations[1,4,16]. In some cases, temperature distributions (in the tabulated data) have been computed from empirical variations of the Crocco integral. In the present study, an objective was to treat the thermal problem independently from a model motivated by any type of Reynolds analogy argument or an empirical version of the Crocco integral. Here a self-consistent structure is presented for the total enthalpy distribution in the boundary layer which is logarithmic in the overlap zone; a formula for the slope of the total enthalpy is derived, as well as a relationship from which the total heat transfer at the wall can be evaluated. The resulting distributions of temperature are then compared directly with the recent experimental data of Carvin[17], as well as other existing data sets[16].

A principal motivation of the present study was to initiate development of embedded-function methods for the computation of high-speed compressible turbulent flows. In the calculation of turbulent flows near walls, a large number of mesh points are required in order to resolve the intense variations that occur in the wall layer in the velocity and temperature distributions. Such grids can put a severe strain on computer resources, even for a two-dimensional flow. For solution approaches based on the full Navier-Stokes equations, the relatively small grid sizes near the surface can also give rise to stability problems in the numerical algorithm. In an attached two-dimensional turbulent flow, the wall layer exhibits an essentially universal and similar behavior; thus, to a large extent, expending a major portion of this computation on a known (and unexceptional) wall-layer solution seems wasteful. For three-dimensional flow, the mesh problems are even more acute, but recent asymptotic analyses[18,19] of three-dimensional turbulent flows are strongly suggestive that a generic (but more complicated) wall-layer structure exists for attached boundary layers. In view of the computational problems just discussed, there has been an increasing interest in recent times in wall-function methods[8] in which a numerical solution is patched at the first grid point from the wall to some form of the "law of the wall"; this procedure obviates the need for a densely packed mesh near the surface, and, in principle, is much more efficient. A more refined procedure has recently been under development by Wahls et al.[20] and Barnwell and Wahls[21]; in this approach, the question of compressibility is addressed directly and a combination of a law of the wall and a "law of the wake" is used to represent the velocity distribution above the overlap zone (in the region where the eddy viscosity is linear in conventional fully numerical methods).

Another related approach is the embedded-function method. Recently, an efficient and accurate algorithm for the computation of mean velocity and temperature profiles in subsonic two-dimensional turbulent boundary layers has been described by Walker, Werle and Ece[22]. The basic method is a semi-analytical embedded-function scheme in which the mean velocity and temperature profiles are represented by smooth analytical functions throughout the wall layer; this is in contrast to previous wall-function methods which simply attempt to tie onto some form of the logarithmic law at the first mesh point off the wall. The present profile models are derived through consideration of the observed coherent

structure and dynamical features of the time-dependent wall-layer flow[15,23]. In the computational algorithm[22], the wall-layer profiles are smoothly matched to the outer-region numerical solutions of the turbulent boundary-layer equations as the calculation proceeds in the downstream direction. Results were compared with those obtained using a conventional approach, in which a solution was computed all the way to the wall using a large number of clustered grid points and an inner region mixing length model with a Van Driest damping factor[1]. In the embedded-function method[22], simple outer region turbulence models are used and the analytic functionals provide the turbulence model for the wall layer; thus, inner models involving the Van Driest damping factor are no longer needed. Calculations were carried out for incompressible and for low-speed subsonic compressible flows; it was determined that up to a 50% reduction in the total mesh points could be achieved, as compared to a conventional method that computes all the way to the wall, with no degradation in accuracy. In addition, since turbulence models and a numerical solution are only required for the outer region, the algorithm is very efficient[22]. At any streamwise location, skin friction and heat-transfer coefficients are calculated through a set of algebraic matching conditions, which are the mathematical statements that the outer region numerical solutions should join smoothly onto the embedded wall-layer functions. Direct comparisons[22] with experimental data for measured heat transfer rates showed excellent agreement.

The work described in this paper represents a first step toward extending the embedded-function methodology to the computation of turbulent supersonic flows. It is worthwhile to note that this type of approach (or any other wall-function method which is tied to a logarithmic profile variation) can only be sensibly applied to an attached turbulent flow. As a turbulent flow separates, it is well known that the logarithmic behavior in the velocity profile disappears. Although there is some evidence that there may be a logarithmic portion of the profile in the back-flow region beyond the separation point, it is evidently a far different functional form than in the upstream boundary layer[24]. This is simply an indication that the physics in the back-flow zone are different from the well-documented behavior of the attached wall layer. For this reason, any attempt to force a wall-function approach, without substantial modification, into a region of separation would not seem to be well conceived. Although this is an area requiring additional modeling, it is also important to appreciate that in most practical flow problems, the turbulent boundary layer is attached over a large portion of the total surface.

From a modeling standpoint, the supersonic turbulent boundary layer is considerably more complex than the subsonic regime, in view of the substantial density variations that occur across the boundary layer. In addition, the asymptotic behavior of the relevant flow quantities is not firmly established, particularly near the overlap zone and in the wall layer; unfortunately, data for the velocity profile within this zone are sparse and often of uncertain reliability. Finally, an objective of the present research is to model the thermal problem directly and in a manner which is independent of the turbulent Prandtl number concept. Unfortunately, unlike subsonic flows, there is a very small data base of temperature surveys for supersonic flow with heat transfer and measurements near the overlap zone are very rare. A substantial portion of supersonic data has been taken with an adiabatic wall, and thus is not useful for direct modeling of the heat transfer problem.

Because the embedded-function approach involves the smooth joining of an exterior numerical solution to a set of functionals, which are logarithmic near the surface, the numerical algorithms involved are not straightforward. A crucial step in the methodology is the determination of the correct asymptotic scaling laws for the velocity and total enthalpy in the overlap zone. This is carried out in the present paper through the development of asymptotic expansions, which describe the structure of the solution of the compressible boundary-layer equations for large Reynolds number. The analysis is in terms of the Howarth-Dorodnitsyn variable which implicitly incorporates the influence of mean density variations across the boundary layer and is believed to be the appropriate normal variable for compressible turbulent flow. The asymptotic results reveal a deficiency in the conventional form of outer-region algebraic models, now in common use, and a modification to account for density variations is proposed. The turbulence models used in the present study for the outer region are simple eddy viscosity and eddy conductivity models and are similar to the Cebeci-Smith[1] and Baldwin-Lomax[2] models; they have been selected here as the simplest possible outer algebraic models in order to demonstrate the concepts involved. For the wall layer, a set of embedded functions for velocity and total enthalpy is given, as well as matching conditions in the overlap zone from which skin-friction and heat-transfer coefficients can be found. In order to test the results of the asymptotic theory, as well as the new turbulence models, a limiting case is considered corresponding to self-similar profiles that evolve in a constant pressure flow with heat transfer; in this situation, the governing equations in the outer region of the boundary layer reduce to ordinary differential equations, for which exact analytical solutions are found. The outer-layer profiles were then matched to the embedded wall-layer functionals to form a set of composite profiles of velocity and total enthalpy across the entire boundary layer. These profiles were then compared directly with experimental data over a range of a Mach numbers and the agreement is very encouraging.

The plan of the paper is as follows. In §2, the governing equations for the compressible turbulent boundary layer are described in terms of the Howarth-Dorodnitsyn variable. A general analysis of the leading-order wall layer is given in §3 while the outer layer is discussed in §4. The compressible turbulence models for the outer layer are described in §5. In §6, the special set of profiles for velocity and total enthalpy in a constant pressure flow are given, and the detailed comparisons with experimental data are discussed in §7.

2. Governing Equations

In this section, the basic equations governing a two-dimensional (or axisymmmetric) nominally steady turbulent boundary-layer flow are summarized. An orthogonal coordinate system (s^*, n^*) is selected, where s^* measures distance along the contour of the wall and n^* is the coordinate in the direction normal to the wall; the corresponding time-mean velocity components are u^* and v^*. Here and throughout the paper an asterisk superscript is used to denote a dimensional quantity. The mean total enthalpy H^* is defined in terms of u^* and the mean static temperature T^* by

$$H^* = C_p^* T^* + \tfrac{1}{2} u^{*2}, \tag{2.1}$$

where C_p^* is the specific heat at constant pressure and is assumed to be constant. Dimensionless variables are defined using a reference length L_{ref}^*, a velocity U_{ref}^*, a viscosity μ_{ref}^* and a density ρ_{ref}^*; in addition T^* and H^* are made dimensionless with respect to a reference temperature T_{ref}^* and $C_p^* T_{ref}^*$ respectively[1]. The dimensionless total enthalpy is therefore given by

[1]This choice of dimensionless variables for the thermal quantities varies somewhat from References 22 and 25, where the explicit choice $T_{ref}^* = U_e^{*2}/C_p^*$ was used; for low speed flows, the latter choice of T_{ref}^* gives unreasonably low temperatures. Thus there are some minor notational differences from Reference 25 in this paper.

$$H = T + \frac{(\gamma-1)}{2} M_{ref}^2 u^2, \tag{2.2}$$

where the reference Mach number is defined by

$$M_{ref}^2 = \frac{U_{ref}^{*2}}{\gamma R T_{ref}^*}, \tag{2.3}$$

$\gamma = C_p^*/C_v^*$ is the ratio of specific heats, and R is the gas constant. Lastly, the pressure is made dimensionless with respect to $\rho_{ref}^* U_{ref}^{*2}$. The governing equations are then:

$$\frac{\partial}{\partial s}(r\rho v) + \frac{\partial}{\partial n}(r\rho v) = 0, \tag{2.4}$$

$$\rho u\frac{\partial u}{\partial s} + \rho v\frac{\partial u}{\partial n} = -\frac{dp_e}{ds} + \frac{\partial \tau}{\partial n}, \tag{2.5}$$

$$\rho u\frac{\partial H}{\partial s} + \rho v\frac{\partial H}{\partial n} = \frac{\partial q}{\partial n}. \tag{2.6}$$

For a two-dimensional plane flow r = 1, while r = r(s) is the dimensionless radius of revolution for an axisymmetric body. In these equations, τ and q are the total stress and a flux defined by

$$\tau = \sigma + \frac{\mu}{Re}\frac{\partial u}{\partial n}, \tag{2.7}$$

$$q = \phi + \frac{(\gamma-1) M_{ref}^2 \mu}{2Re}\frac{\partial}{\partial n}(u^2) + \frac{\mu}{PrRe}\left[\frac{\partial H}{\partial n} - \frac{(\gamma-1)}{2} M_{ref}^2 \frac{\partial}{\partial n}(u^2)\right], \tag{2.8}$$

where σ and ϕ are the Reynolds stress and turbulent flux given by

$$\sigma = -\rho\overline{u'v'}, \qquad \phi = -\rho\overline{v'H'}, \tag{2.9}$$

and the Reynolds number Re and Prandtl number Pr are defined by

$$Re = \frac{\rho_{ref}^* U_{ref}^* L_{ref}^*}{\mu_{ref}^*}, \qquad Pr = \frac{\mu^* C_p^*}{k^*}. \tag{2.10}$$

Here μ^* and k^* are the (dimensional) absolute viscosity and thermal conductivity, respectively, and although a variable Prandtl number is permissible in equation (2.8), Pr will generally be assumed constant.

The pressure is independent of n across the boundary layer and equal to the value $p_e(s)$ at the boundary-layer edge; equation (2.5) becomes

$$\frac{dp_e}{ds} = -\rho_e U_e \frac{dU_e}{ds}, \tag{2.11}$$

which is equivalent to the Bernoulli equation for steady compressible flow. The subscript e is used throughout to denote a variable evaluated at the boundary-layer edge where the free-stream velocity $U_e(s)$, static temperature $T_e(s)$ and density $\rho_e(s)$ are known. The equation of state is taken to be the ideal gas law which (in dimensionless form) is

$$p_e = \rho T/(\gamma M_{ref}^2), \tag{2.12}$$

thereby relating the density and static temperature across the boundary layer to $p_e(s)$. Lastly, the viscosity μ is taken to be a function of temperature alone and obtained from the Sutherland relation

$$\frac{\mu}{\mu_w} = \left(\frac{T}{T_w}\right)^{3/2}\left(\frac{T_w + S}{T + S}\right), \tag{2.13}$$

where $S = S^*/T_{ref}^*$ and the constant S^* has the value 199° R for air. Here and throughout a subscript w is used to denote a quantity evaluated at the wall.

It is possible to remove the density from most of the terms in the governing equations (2.4) to (2.6) by introducing the Howarth-Dorodnitsyn transformation[26]

$$Y = \int_0^n \rho dn, \qquad \tilde{v} = \rho v + u\frac{\partial Y}{\partial s}. \tag{2.14}$$

Here Y measures a density-weighted distance from the wall. It is easily shown that equations (2.4) to (2.8) become

$$\frac{\partial}{\partial s}(ru) + \frac{\partial}{\partial Y}(r\tilde{v}) = 0, \tag{2.15}$$

$$u\frac{\partial u}{\partial s} + \tilde{v}\frac{\partial u}{\partial Y} = -\frac{\rho_e}{\rho} U_e \frac{dU_e}{ds} + \frac{\partial \tau}{\partial Y}, \tag{2.16}$$

$$u\frac{\partial H}{\partial s} + \tilde{v}\frac{\partial H}{\partial Y} = \frac{\partial q}{\partial Y}, \tag{2.17}$$

where the total stress and flux are

$$\tau = \sigma + \frac{\mu\rho}{Re}\frac{\partial u}{\partial Y}, \tag{2.18}$$

$$q = \phi + \frac{(\gamma-1)}{2Re} M_{ref}^2 \mu\rho \frac{\partial}{\partial Y}(u^2) + \frac{\mu\rho}{PrRe}\left[\frac{\partial H}{\partial Y} - \frac{(\gamma-1)}{2} M_{ref}^2 \frac{\partial}{\partial Y}(u^2)\right] \tag{2.19}$$

respectively. The boundary conditions are:

$$u = v = \tilde{v} = 0 \text{ at } Y = 0; \qquad u \to U_e \text{ as } Y \to \infty, \tag{2.20}$$

$$H = H_w \text{ at } Y = 0, \quad H \to H_e \text{ as } Y \to \infty, \tag{2.21}$$

or, for an adiabatic wall,

$$\frac{\partial H}{\partial Y} = 0 \text{ at } Y = 0. \tag{2.22}$$

For steady flow, H_e is a constant and the Mach number in the mainstream is related to H_e and U_e by

$$U_e^2 = \frac{\alpha H_e}{(\gamma-1)M_{ref}^2}, \tag{2.23}$$

where α is defined by

$$\alpha = \frac{(\gamma-1)M_e^2}{1 + (\frac{\gamma-1}{2})M_e^2}. \tag{2.24}$$

The density and absolute viscosity are related to the static temperature T through equations (2.12) and (2.13) and it is easily shown that the temperature is related to H and u by

$$\frac{T}{T_e} = \left\{1 + \frac{\gamma-1}{2}M_e^2\right\}\left\{\frac{H}{H_e} - \tfrac{1}{2}\,\alpha\,\frac{u^2}{U_e^2}\right\}. \tag{2.25}$$

Furthermore, since the pressure does not vary, to leading order across the boundary layer at any fixed streamwise location, it follows from equation (2.12) that

$$\frac{\rho_e}{\rho} = \frac{T}{T_e}. \tag{2.26}$$

Therefore the density ratio in equation (2.16) may be replaced by the right side of equation (2.25) and the compressible problem is expressed solely in terms of the unknowns u, $\tilde{v}$ and H. It is noted in passing that using equation (2.21), it is easily shown that equation (2.25) may be rewritten in the form

$$\frac{T}{T_w} = \frac{H_e}{H_w}\left\{\frac{H}{H_e} - \tfrac{1}{2}\,\alpha\,\frac{u^2}{U_e^2}\right\}. \tag{2.27}$$

Simpler subsets of these governing equations in the limit of large Reynolds number will now be identified.

3. The Wall Layer

Consider first the wall layer and define the dimensionless friction velocity u_τ according to

$$u_\tau^2 = \frac{\mu_w}{\rho_w Re}\left.\frac{\partial u}{\partial n}\right|_{n=o}. \tag{3.1}$$

A number of studies[23,25,27-29] have identified the length and velocity scales in the wall layer in the limit $Re \to \infty$. If Δ_i denotes the length scale associated with the inner wall layer, it is easily shown for incompressible flow that

$$\Delta_i = O(\log Re/Re), \qquad u_\tau/U_e = O(1/\log Re), \tag{3.2}$$

as $Re \to \infty$. For the compressible flow of interest in this paper, the scaled wall-layer variable is defined by

$$Y^+ = \frac{Y}{\Delta_i}, \qquad \Delta_i = \frac{\mu_w}{u_\tau Re}. \tag{3.3}$$

It should be noted that the appropriate scaling laws for compressible turbulent flow have been controversial and a number of relations have been proposed (see, for example, References 1, 4, and 10). For the specific choice adopted here, it is worthwhile to note that very close to the wall (from equation (2.14)) $Y \simeq n\rho_w$ and the normal variable defined in equation (3.3) reduces to

$$Y^+ \sim \frac{\rho_w u_\tau\, Re\, n}{\mu_w} = \frac{\rho_w^* u_\tau}{\mu_w^*}\, n^*, \tag{3.4}$$

as $n \to 0$; thus, equation (3.4) is the conventional definition of the variable y^+ in terms of actual physical distance from the wall. Elsewhere in the wall layer, a density variation is contained implicitly within the scaled normal variable through the definiton of Y in equation (2.14).

It is well known[14,23,27-29] that, since the wall layer is thin and the streamwise velocity is $O(u_\tau)$ (and hence small), the dominant terms in equation (2.5) are the viscous and Reynolds stress terms; in the limit as $Re \to \infty$ both the convective terms and the pressure gradient are negligible to leading order in the wall layer. This feature of the wall layer is discussed extensively elsewhere[14,23,27-29] but may easily be checked using the scalings that will be adopted here. Equation (2.16) reduces to

$$\frac{\partial \tau}{\partial Y^+} = 0, \tag{3.5}$$

or using equation (2.18)

$$u_\tau \frac{\partial}{\partial Y^+}\left\{\frac{\mu\rho}{\mu_w}\frac{\partial u}{\partial Y^+}\right\} + \frac{\partial \sigma}{\partial Y^+} = 0. \tag{3.6}$$

Integrating this equation form 0 to Y^+ and using equation (3.1) as well as the fact that $\sigma = 0$ at $Y^+ = 0$, it follows that

$$\tau = u_\tau \frac{\mu\rho}{\mu_w}\frac{\partial u}{\partial Y^+} + \sigma = \rho_w u_\tau^2, \tag{3.7}$$

and therefore the total stress $\tau = \rho_w u_\tau^2$ across the wall layer, to leading order. The velocity u is logarithmic for Y^+ large and as $Y^+ \to \infty$, the viscous stress term in equation (3.7) becomes small and

$$\sigma \to \rho_w u_\tau^2 \text{ as } Y^+ \to \infty, \tag{3.8}$$

to leading order. It should be noted that any model which is adopted for the Reynolds stress in the outer layer must conform to the behavior indicated by equation (3.8) in the overlap zone.

In view of equations (3.7) and (3.8), the velocity and Reynolds stress in the wall layer are expanded as

$$u = u_\tau\, U^+(Y^+) + \ldots, \quad \sigma = \rho_w u_\tau^2\, \sigma_1(Y^+) + \ldots, \tag{3.9}$$

where U^+ and σ_1 are profile functions, one of which must be specified in order to define a specific closure model, subject to the conditions that

$$\frac{\partial U^+}{\partial Y^+} = 1, \qquad U^+ = 0, \qquad \sigma_1 = 0 \quad \text{at} \quad Y^+ = 0, \tag{3.10}$$

and

$$U^+ \sim \tfrac{1}{\kappa}\log Y^+ + C_i, \quad \sigma_1 \to 1 \text{ as } Y^+ \to \infty. \tag{3.11}$$

In the above logarithmic law, κ is the von Karman constant and C_i is the inner log-law constant, usually assumed to have universal values of $\kappa = 0.41$ and $C_i = 5.0$. Equation (3.7) becomes

$$\frac{\mu\rho}{\mu_w\rho_w}\frac{\partial U^+}{\partial Y^+} + \sigma_1 = 1. \tag{3.12}$$

It can be shown (Appendix A) that the Sutherland relation (2.13) is consistent with the Chapman-Rubesin law $\mu\rho = \mu_w\rho_w$ in the wall layer and hence equation (3.12) becomes

$$\frac{\partial U^+}{\partial Y^+} + \sigma_1 = 1. \tag{3.13}$$

In view of the fact that the convective terms do not play a role in the leading-order wall-layer equations, the dependence of the wall-layer solution on the streamwise variable s can at most be parametric and σ_1 and U^+ are functions of Y^+ alone. In the present study, the turbulence model used for the inner layer is the wll-layer model developed by Walker et al.[23], which is based on the coherent structure of the near-wall flow. Through consideration of typical motions during a typical cycle in the wall layer, an expression for the mean-profile is produced[23] via a time-average over the representative cycle. The result is an analytic function $U^+(Y^+)$ (which also contains an explicit dependence on the average burst period). This functional satisfies the first of conditions (3.10) and (3.11) and provides a formula for U^+ across the entire wall layer. A summary of the function U^+ is given in Appendix C. It is noted in passing that an expression for the Reynolds stress function σ_1 can readily be obtained from equation (3.13) and that direct comparison[23] with measured Reynolds stress data shows excellent correspondence with the theoretical expression.

Now consider the thermal problem. Again it is easily shown that the convective terms are negligible to leading order in the wall layer; equation (2.17) reduces to

$$\frac{\partial q}{\partial Y^+} = 0, \tag{3.14}$$

and consequently $q = q_w$ is invariant, to leading order, across the wall layer. It follows from equation (2.19) that

$$q_w = \phi + (\gamma\text{-}1)M_{ref}^2\frac{\mu\rho}{\rho_w}u_\tau u\frac{\partial u}{\partial Y^+} + \frac{u_\tau\mu\rho}{Pr\mu_w}\frac{\partial H}{\partial Y^+}$$

$$- (\gamma\text{-}1)M_{ref}^2\frac{\mu\rho}{\rho_w Pr}u_\tau u\frac{\partial u}{\partial Y^+}. \tag{3.15}$$

But since $u = \phi = 0$ at $Y^+ = 0$, it follows that

$$q_w = \frac{u_\tau\rho_w}{Pr}\left.\frac{\partial H}{\partial Y^+}\right|_{Y^+=0}, \tag{3.16}$$

and consequently q_w denotes a dimensionless heat flux at the wall defined by

$$q_w = \frac{q_w^*}{\rho_{ref}^* U_{ref}^* C_p^* T_{ref}^*}, \quad q_w^* = k_w^*\left.\frac{\partial T^*}{\partial n^*}\right|_{n^*=0}, \tag{3.17}$$

where k_w^* is the dimensional thermal conductivity of the fluid at the wall. Note that q_w denotes a heat flux from *fluid to the wall* (see Appendix B).

It will subsequently be shown (in §4) that q_w is $O(u_\tau^2/U_e^2)$ and since u is $O(u_\tau)$ (c.f. equations (3.9)), it is easily shown that the second and fourth terms in equation (3.15), namely the viscous dissipation term and a portion of the conduction term, are negligible to leading order provided $(u_\tau/U_e) << 1$. The form of equation (3.15) then suggests the following expansions for the turbulence term and total enthalpy in the wall layer:

$$\phi = q_w\,\phi_1 + \cdots, \tag{3.18}$$

$$H = H_w + \frac{q_w}{\rho_w u_\tau}\theta^+ + \cdots, \tag{3.19}$$

where ϕ_1 and θ^+ are functions of Y^+. Upon substitution in equation (3.15), it follows that to leading order

$$\frac{1}{Pr}\frac{\mu\rho}{\mu_w\rho_w}\frac{\partial\theta^+}{\partial Y^+} + \phi_1 = 1. \tag{3.20}$$

The profile function θ^+ is logarithmic for large Y^+ and thus as $Y^+ \to \infty$, the first term in equation (3.20) (corresponding to conduction) approaches zero. Therefore,

$$\phi_1 \to 1 \quad \text{as } Y^+ \to \infty, \tag{3.21}$$

or equivalently

$$\phi \to q_w \quad \text{as } Y^+ \to \infty. \tag{3.22}$$

Again, any model for the turbulent heat flux in the outer layer must conform to the behavior indicated in equation (3.22) in the overlap zone.

In the present study, the turbulence model used for the inner layer is the wall-layer model developed by Walker, Scharnhorst and Weigand[15], which is based on the coherent structure of the near wall flow and the transport of thermal energy during a typical wall-layer cycle. The analysis[14,15] produces a functional which exhibits a dependence on the square root of the Prandtl number (as well as the mean burst period) and

$$\theta^+ = \theta^+(Y_\theta^+), \quad Y_\theta^+ = \sqrt{Pr}\,Y^+. \tag{3.23}$$

Expressed in terms of the variable Y_θ^+ and again using the Chapman-Rubesin relation (Appendix A), equation (3.20) becomes

$$\frac{1}{\sqrt{Pr}}\frac{\partial\theta^+}{\partial Y_\theta^+} + \phi_1 = 1. \tag{3.24}$$

The functional θ^+ is similar[15] in form to U^+ and

$$\theta^+ = 0, \quad \frac{d\theta^+}{dY_\theta^+} = \sqrt{Pr}, \quad \text{at } Y^+ = 0, \tag{3.25}$$

$$\theta^+ \sim \frac{1}{\kappa_\theta}\log Y_\theta^+ + B_i, \quad \text{as } Y_\theta^+ \to \infty. \tag{3.26}$$

Here κ_θ plays the role of the von Karman constant in the velocity distribution, but κ_θ is not constant in general and depends on local flow conditions[14,15]. Formulae for the constant B_i and κ_θ will be discussed subsequently. The function θ^+ is described in Appendix C.

4. The Outer Layer

In the outer layer, variations in the streamwise direction affect the solution structure directly, and it is convenient to define new independent variables by the Mangler transformation

$$\xi = \int_o^s r^2\, ds, \quad \eta = \frac{rY}{\Delta_o}, \tag{4.1}$$

where Y is the Howarth-Dorodnitsyn variable defined in equation (2.14) and $\Delta_o(\xi, Re)$ is a scale proportional to the local boundary-layer thickness, which will be selected subsequently. The following new dependent variables are introduced,

$$F = \frac{u}{U_e}, \quad V = \frac{1}{r\Delta_o U_e}\left\{\tilde{v} - \eta u \frac{\partial}{\partial s}\left(\frac{\Delta_o}{r}\right)\right\}, \quad I = \frac{H}{H_e}, \tag{4.2}$$

where $\tilde{v}$ is the normal velocity defined in equation (2.14); alternatively, V may be expressed in terms of the original velocity v (c.f. equations (2.4) - (2.6)) according to

$$V = \frac{1}{r^2}\left\{\frac{r\rho v}{\Delta_o U_e} + \frac{\partial \eta}{\partial s}\Big|_n F\right\}. \tag{4.3}$$

It can then be shown that either of equations (2.4)-(2.6) or (2.15)-(2.17) become

$$\frac{\partial}{\partial \xi}(\Delta_o U_e F) + \frac{\partial}{\partial \eta}(\Delta_o U_e V) = 0, \tag{4.4}$$

$$F\frac{\partial F}{\partial \xi} + V\frac{\partial F}{\partial \eta} = \frac{1}{M_e}\frac{dM_e}{d\xi}(I - F^2) + \frac{1}{\Delta_o r U_e^2}\frac{\partial \tau}{\partial \eta}, \tag{4.5}$$

$$F\frac{\partial I}{\partial \xi} + V\frac{\partial I}{\partial \eta} = \frac{1}{\Delta_o r U_e H_e}\frac{\partial q}{\partial \eta}, \tag{4.6}$$

where M_e is the local mainstream Mach number.

In the outer layer, the solutions for F and I are in the form of a defect law and guided by the inner expansions in equations (3.9), (3.18) and (3.19), the outer expansions are written in the form

$$F = 1 + \frac{u_\tau}{U_e}\frac{\partial F_1}{\partial \eta} + \dots, \tag{4.7}$$

$$I = 1 + \frac{q_w}{\rho_w u_\tau H_e}\Theta_1 + \dots, \tag{4.8}$$

where F_1 and Θ_1 are functions of (ξ,η) to be determined. A stream function may be defined by

$$\frac{\partial \psi}{\partial \eta} = \Delta_o U_e F, \quad \frac{\partial \psi}{\partial \xi} = -\Delta_o U_e V, \tag{4.9}$$

in order to satisfy equation (4.4) identically and using equation (4.7), it follows that ψ has the expansion

$$\psi = \Delta_o U_e \eta + \Delta_o u_\tau F_1(\xi, \eta) + \dots. \tag{4.10}$$

Thus V is given by

$$V = -\frac{(\Delta_o U_e)'}{\Delta_o U_e}\eta - \frac{1}{\Delta_o U_e}\frac{\partial}{\partial \xi}(\Delta_o u_\tau F_1) + \dots, \tag{4.11}$$

where the prime denotes differentiation with respect to ξ. In the expansions (4.7) and (4.8), the gauge functions will be denoted by

$$u_* = \frac{u_\tau}{U_e}, \quad q_* = \frac{q_w}{\rho_w u_\tau H_e}. \tag{4.12}$$

The matching with the inner layer will shortly establish that Δ_o and q_* are $O(u_*)$ and also that

$$\frac{du_*}{d\xi} = O(u_*^2), \quad u_* \to 0 \text{ as } Re \to \infty. \tag{4.13}$$

Using these results and substituting the expansions (4.7), (4.8) and (4.11) into equations (4.5) and (4.6) yields, for an isothermal wall and to leading order,

$$\frac{\partial^2 F_1}{\partial \xi \partial \eta} - \frac{(\Delta_o U_e)'}{\Delta_o U_e}\eta\frac{\partial^2 F_1}{\partial \eta^2} = \frac{1}{M_e}\frac{dM_e}{d\xi}\left\{\frac{q_*}{u_*}\Theta_1 - 2\frac{\partial F_1}{\partial \eta}\right\} + \frac{1}{r\Delta_o U_e u_\tau}\frac{\partial \tau}{\partial \eta}, \tag{4.14}$$

$$\frac{\partial \Theta_1}{\partial \xi} - \frac{(\Delta_o U_e)'}{\Delta_o U_e}\eta\frac{\partial \Theta_1}{\partial \eta} = \frac{1}{r\Delta_o U_e H_e q_*}\frac{\partial q}{\partial \eta}. \tag{4.15}$$

The boundary conditions associated with these equations are

$$\frac{\partial F_1}{\partial \eta}, \ \Theta_1 \to 0, \quad \text{as } \eta \to \infty. \tag{4.16}$$

and

$$\frac{\partial F_1}{\partial \eta} \sim \frac{1}{\kappa}\log \eta + C_o, \quad \text{as } \eta \to 0, \tag{4.17}$$

$$\Theta_1 \sim \frac{1}{\kappa_\theta}\log \eta + B_o, \quad \text{as } \eta \to 0. \tag{4.18}$$

The limiting behavior in equations (4.17) and (4.18) ensure the existence of a logarithmic overlap region between the inner and outer layers. Note that the general form of conditions (4.17) and (4.18) applies for an attached turbulent boundary-layer flow and is independent of any specific turbulence closure; C_o and B_o are, in general, functions of ξ (to be found) and the actual streamwise distribution of these quantitites is strongly influenced by the particular outer-region turbulence model adopted. Although $\kappa = 0.41$ is constant over a wide range of flow conditions, there is no universally agreed upon constant value of κ_θ, and careful comparisons[14] with measured temperature profile data in low-speed subsonic boundary layers show that κ_θ depends on local flow conditions. A formula for κ_θ will now be developed.

Matching of the velocity profile in the overlap zone is carried out using the asymptotic forms in equations (3.11) and (4.17) and leads to the matching condition

$$\frac{U_e}{u_\tau} = \frac{1}{\kappa}\log\left\{\frac{\Delta_o Re\, u_\tau}{r\mu_w}\right\} + C_i - C_o. \tag{4.19}$$

For a known wall viscosity and Reynolds number, equation (4.19) provides a relation to determine the friction velocity u_τ, based on the inner-layer constant C_i and the characteristics of

the outer layer profile which enter through the outer scale Δ_o and C_o. It is noted in passing that the results quoted in equations (3.2) and (4.13) are readily confirmed using equation (4.19). Matching of the total enthalpy profile using the asymptotic forms (3.26) and (4.18) yields

$$\frac{(1 - I_w)}{q_*} = \frac{1}{\kappa_\theta} \log \left\{ \frac{\Delta_o Re\, u_\tau \sqrt{Pr}}{r \mu_w} \right\} + B_i - B_o. \tag{4.20}$$

where

$$I_w = H_w / H_e. \tag{4.21}$$

In the limit of large Reynolds number, the logarithmic terms on the right side of equations (4.19) and (4.20) dominate, and it follows that

$$\frac{\kappa_\theta}{\kappa} \sim \frac{q_*}{(1 - I_w) u_*} \quad \text{as} \quad Re \to \infty. \tag{4.22}$$

In this paper, the value of κ_θ is assumed to be defined by the asymptotic result in equation (4.22), and combining equations (4.19), (4.20), and (4.22), it is easily shown that

$$\frac{\kappa_\theta}{\kappa} = \frac{C_i - C_o - \frac{1}{2\kappa} \log Pr}{B_i - B_o}. \tag{4.23}$$

The thermal match condition (4.20) serves to determine the heat-transfer parameter q_* for given values of Prandtl number, wall temperature, and u_τ; the characteristics of the outer- and inner-layer profiles enter through the log-law parameters B_o, C_o and B_i, C_i respectively. In practice, the relations (4.20) - (4.23) can be utilized in one of two ways, both of which are essentially equivalent. In the first approach[14], κ_θ is calculated from equation (4.22) (with $\kappa = 0.41$) for a given estimate of q_* and u_*, and then q_* is updated using the full match condition (4.20); both quantities are then refined through an obvious iteration. In the second approach, which was used here, κ_θ is calculated directly from equation (4.23) and q_* is then evaluated from equation (4.22). In the turbulence models that will be adopted in the present study (c.f. section 5), both B_o and B_i are implicit functions of κ_θ and, consequently, equation (4.23) is a nonlinear equation for κ_θ which is solved iteratively.

It should be noted that q_* may be expressed in terms of a Stanton number defined by

$$St = \frac{q_w^*}{\rho_w^* U_e^* (H_e^* - H_w^*)} = \frac{q_w}{\rho_w U_e (H_e - H_w)}, \tag{4.24}$$

and it is easily shown that

$$St = \frac{q_* u_*}{(1 - I_w)}. \tag{4.25}$$

In terms of Stanton number, equation (4.22) gives

$$\kappa_\theta = \kappa\, St / u_*^2. \tag{4.26}$$

One potential disadvantage associated with the use of Stanton number in a high speed compressible flow occurs with a heated wall when H_w is close to H_e and thus St is very large. An alternative heat transfer parameter[16] Q_w, which avoids the difficulty, may be defined by

$$Q_w = \frac{q_w^*}{\rho_w^* U_e^* H_e^*} = \frac{q_w}{\rho_w U_e H_e}. \tag{4.27}$$

It follows that $Q_w = q_* u_*$ and equation (4.22) becomes

$$\frac{\kappa_\theta}{\kappa} = \frac{Q_w}{(1 - I_w)\, u_*^2}. \tag{4.28}$$

Whether St or Q_w is used as the basic heat transfer parameter is a matter of preference.

5. Turbulence Models

The turbulence models used for the outer layer are relatively simple eddy viscosity and eddy conductivity models similar to the Cebeci-Smith[1] or the Baldwin-Lomax[2] outer models. However, it is important to appreciate that the latter models were primarily developed and refined for low-speed flows; consequently, the arbitrary extension of these models to the prediction of high-speed compressible flows is questionable. On the other hand, an attractive feature of algebraic models is their relative simplicity, and it is of interest to develop such an approach which adequately accounts for the effects of compressibility. In general, such models are of the form

$$\tau = \rho \epsilon \frac{\partial u}{\partial n}, \quad q = \rho \epsilon_H \frac{\partial H}{\partial n}, \tag{5.1}$$

where ϵ and ϵ_H are the total effective viscosity and conductivity, respectively. Throughout most of the outer layer, τ and q consist primarily of Reynolds stress and turbulent flux. Consider first the eddy viscosity function. In terms of the Howarth-Dorodnitsyn variable Y defined in equation (2.14) or the scaled outer variable defined in equation (4.1)

$$\tau = \rho^2 \epsilon \frac{\partial u}{\partial Y} = \frac{\rho^2 \epsilon r}{\Delta_o} \frac{\partial u}{\partial \eta}. \tag{5.2}$$

But in the outer layer, u is in the form of a defect law (c.f. equation (4.7)) and, according to equation (4.17) is logarithmic for small η. It follows that

$$\tau \sim \frac{\rho^2 \epsilon r u_\tau}{\Delta_o \kappa \eta} = \frac{\rho^2 \epsilon u_\tau}{\kappa Y}, \quad \text{as} \quad \eta \to 0. \tag{5.3}$$

But from equation (3.7)

$$\tau \sim \rho_w u_\tau^2, \quad \text{as} \quad Y^+ \to \infty, \tag{5.4}$$

and it follows that in order to provide a smooth transition between the inner and outer layer, the eddy viscosity function must have the following form for small η

$$\epsilon \sim \frac{\rho_w}{\rho^2} u_\tau \kappa Y = \frac{\rho_w}{\rho^2} \frac{u_\tau \Delta_o}{r} \kappa \eta, \quad \text{as} \quad \eta \to 0. \tag{5.5}$$

The linear form in Y contained in equation (5.5) is a necessary feature of all proper outer-region models and is necessary to produce the logarithmic behavior in the mean profile. The important aspect of equation (5.5) is the functional dependence on the density. For larger values of Y, the linear dependence on Y must be modified and simple far-field eddy

viscosity formulae, for low-speed compressible flow, are

$$\epsilon_o = KU_e\delta^*, \tag{5.6}$$

for the Cebeci-Smith model[1] and

$$\epsilon_o = c_p\ K\ y_{max}\ \tilde{F}_{max}, \tag{5.7}$$

for the Baldwin-Lomax model[2]. In these formulae, K is a constant which normally has the value K = 0.0168, and δ^* is the incompressible displacement thickness defined by

$$\delta^* = \int_0^\infty \left\{1 - \frac{u}{U_e}\right\} dn. \tag{5.8}$$

For the Baldwin-Lomax model, y_{max} is the physical location where the function $\tilde{F} = y|\partial u/\partial y|$ achieves a maximum and $\tilde{F}_{max}$ is the corresponding value of $\tilde{F}$; c_p is a constant (having a value of about 1.6) which has been adjusted[2] so that the model produced essentially similar results to the Cebeci-Smith model at low Mach numbers. The linear variation of the eddy viscosity for small η is normally joined to either of (5.6) or (5.7) as a simple ramp function, with the juncture being determined by the location where the two formulae give the same value.

For compressible flow, a corresponding simple formulation is desired. Two requirements for such a model are that it behave according to equation (5.5) for small η and also that the far-field portion of the model should reduce to either equation (5.6) or (5.7) for low Mach numbers. Unfortunately, there is a wide variety of functional forms that would fulfill both of these requirements. A number of formulae were tested in this study by producing profiles which could be compared directly with experimental data. One additional consideration relative to model selection was that the adopted form should represent the situation well over a range of Mach numbers without introducing additional empiricism. Here the modification of the Cebeci-Smith-type model will be given and an equivalent form for the Baldwin-Lomax model (which gives essentially equivalent results) can be readily inferred. The compressible eddy viscosity formula for the outer layer used in this study is

$$\epsilon = \frac{\rho_w\rho_e}{\rho^2}\ U_e\delta^*\ \hat{\epsilon}(\eta), \tag{5.9}$$

where

$$\hat{\epsilon}(\eta) = \begin{cases} K, & \eta > \eta_m, \\ \kappa\eta/\eta_1, & \eta \le \eta_m, \end{cases} \tag{5.10}$$

where

$$\eta_1 = \frac{r\rho_e U_e\delta^*}{\Delta_o u_\tau}, \quad \eta_m = \frac{K\eta_1}{\kappa}, \quad K = 0.0168. \tag{5.11}$$

The form of ϵ in equation (5.9) was adopted partially for convenience; the factor of ρ^{-2}, mandated by the matching to the wall layer, is carried through the outer layer in order that patch point η_m between the two pieces of the ramp function in equation (5.10) is a function of streamwise distance alone and not η.

Following similar arguments to those used for the eddy-viscosity function, it is easily shown using equation (3.22), (4.18) and (5.1) that the eddy conductivity function ϵ_H must have the following form for small η

$$\epsilon_H \sim \frac{\rho_w}{\rho^2}\ u_\tau\kappa_\ell Y = \frac{\rho_w}{\rho^2}\ \frac{u_\tau\Delta_\ell}{t}\ \kappa_\ell\eta, \qquad \text{as } \eta \to 0. \tag{5.12}$$

For larger values of η, the linear dependence on η must be modified and a simple far-field eddy conductivity formula for low speed subsonic compressible flow is[14,15]

$$\epsilon_{Ho} = K_h\ U_e\ \delta^*. \tag{5.13}$$

Extensive comparisons[14] with experimental data for the temperature profile have shown that for constant pressure flow at subsonic speeds $K_h = 0.0245$. Again, a generalization to high-speed compressible flow is sought which conforms to the condition (5.12) and reduces to equation (5.13) in the outer part of the boundary layer for low Mach numbers. The eddy-conductivity formula used in the present study is consistent with the form of equation (5.9) and is

$$\epsilon_H = \frac{\rho_w\rho_e}{\rho^2}\ U_e\ \delta^*\ \hat{\epsilon}_H(\eta), \tag{5.14}$$

where

$$\hat{\epsilon}_H = \begin{cases} K_h, & \eta > \bar{\eta}_m, \\ \kappa_\ell\eta/\eta_1, & \eta \le \bar{\eta}_m, \end{cases} \tag{5.15}$$

where η_1 is defined by equation (5.11) and

$$K_h = 0.0245, \quad \bar{\eta}_m = K_h\eta_1/\kappa_\ell. \tag{5.16}$$

Upon substituting equations (5.1), (5.9), and (5.14) into (4.14) and (4.15), it is easily shown that

$$\frac{\partial}{\partial\eta}\left\{\hat{\epsilon}\frac{\partial^2 F_1}{\partial\eta^2}\right\} + a(\xi)\eta\frac{\partial^2 F_1}{\partial\eta^2} + b(\xi)\left\{(1 - I_\omega)\frac{\kappa_\ell}{\kappa}\Theta_1 - 2\frac{\partial F_1}{\partial\eta}\right\} = \sigma(\xi)\frac{\partial^2 F_1}{\partial\xi\partial\eta}, \tag{5.17}$$

$$\frac{\partial}{\partial\eta}\left(\hat{\epsilon}_H\frac{\partial\Theta_1}{\partial\eta}\right) + a(\xi)\eta\frac{\partial\Theta_1}{\partial\eta} = \sigma(\xi)\frac{\partial\Theta_1}{\partial\xi}, \tag{5.18}$$

where the coefficients in these equations are given by

$$a(\xi) = \frac{r(\Delta_o U_e)'}{\rho_w\eta_1 u_\tau}, \tag{5.19}$$

$$\sigma(\xi) = \frac{r(\Delta_o U_e)}{\rho_w u_\tau\eta_1}, \tag{5.20}$$

$$b(\xi) = \frac{\sigma(\xi)}{M_e}\frac{dM_e}{d\xi}. \tag{5.21}$$

The turbulence models for the wall layer are the embedded functions which are described in Appendix C. It may be inferred that the profile model U^+ in equation (C.1) contains the following parameters: (a) the von Karman

constant κ, (b) the inner "log-law"constant C_i, (c) the burst period T_B^+, and (d) the parameter t_0^+. These parameters are not independent however and, given any two, the other two parameters may be computed from equations (C.9) and (C.10). For example, for commonly used values of $\kappa = 0.41$ and $C_i = 5.0$, the solution of equation (C.9) and (C.10) gives

$$T_B^+ = 110.2, \quad t_0^+ = 0.00801. \tag{5.22}$$

Other values of κ and/or T_B^+ may be used to produce a different value of C_i. In general, T_B^+ will be large with respect to t_0^+ and an expansion of equations (C.9) and (C.10) for small (t_0^+/T_B^+) yields

$$C_i \sim \tfrac{1}{2}(\pi T_B^+)^{1/2} + \tfrac{1}{\kappa}\left\{1 + \frac{\gamma_0}{2} - \tfrac{1}{2}\log(4T_B^+)\right\} + \ldots, \tag{5.23}$$

to leading order. This gives C_i as an explicit function of κ and T_B^+; the value of C_i may be refined (if desired) by solving equations (C.9) and (C.10) exactly (for given values of κ and T_B^+). For the total enthalpy, the corresponding estimate of B_i is

$$B_i = \tfrac{1}{2}(\pi T_B^+ Pr)^{1/2} + \tfrac{1}{\kappa_\theta}\left\{1 + \frac{\gamma_0}{2} - \tfrac{1}{2}\log(4T_B^+)\right\} + \ldots, \tag{5.24}$$

which also may be refined using equations (C.9) and (C.10).

6. Self-similar Solutions

In this section, a set of self-similar outer layer profiles will be developed using the new outer-region turbulence models given by equations (5.9) and (5.14). These outer-layer functions will subsequently be combined with inner wall-layer profiles to form composite profiles for velocity and total enthalpy across the entire boundary layer. A direct comparison will then be made with measured experimental data in order to validate the turbulence models, as well as the general approach. A large portion of measured profile data in supersonic boundary layers have been taken in constant pressure conditions and, for simplicity, only this situation will be addressed here; solutions for flows with pressure gradient will be considered elsewhere. Solutions of equations (5.17) and (5.18) for which

$$F_1 = F_1(\eta), \quad \Theta_1 = \Theta_1(\eta), \tag{6.1}$$

and M_e is constant ($b = 0$) are now sought. It follows from equation (5.17) that $\hat{\epsilon}$ must be a function of η alone which, from equations (5.10) and (5.11), requires that η_1 be independent of ξ; a second requirement is that $a(\xi)$ is constant. The first requirement may be satisfied by selecting the outer scale Δ_o according to

$$\Delta_o = \frac{r\rho_e U_e \delta^*}{u_\tau}; \tag{6.2}$$

consequently, the two conditions are

$$\eta_1 = 1, \quad a(\xi) = a, \tag{6.3}$$

where a is constant. For similarity in the total enthalpy equation, the additional requirements are, from equation (5.16), that κ_θ must be constant as well as $(q_*/u_*)/(1 - I_w)$ from equation (4.22). Under these circumstances, equations (5.17) and (5.18) reduce to

$$\frac{d}{d\eta}\left\{\hat{\epsilon}\frac{d^2F_1}{d\eta^2}\right\} + a\eta\frac{d^2F_1}{d\eta^2} = 0, \tag{6.4}$$

$$\frac{d}{d\eta}\left\{\hat{\epsilon}_H\frac{d\Theta_1}{d\eta}\right\} + a\eta\frac{d\Theta_1}{d\eta} = 0, \tag{6.5}$$

where $\hat{\epsilon}$ and $\hat{\epsilon}_H$ are given by equations (5.10) and (5.15) but with $\eta_1 = 1$. The solution of equation (6.4) which satisfies conditions (4.16) and (4.17) is given by

$$\frac{dF_1}{d\eta} = \begin{cases} -\sqrt{\frac{\pi}{2Ka}}\, e^{-Ka/2\kappa^2}\, \mathrm{erfc}\left\{\sqrt{\frac{a}{2K}}\eta\right\} & \eta > \eta_m, \\ -\frac{1}{\kappa}E_1\left(\frac{a\eta}{\kappa}\right) + C_o - \frac{1}{\kappa}\left\{\gamma_o - \log\left(\frac{\kappa}{a}\right)\right. & \eta \le \eta_m, \end{cases} \tag{6.6}$$

where C_o is the outer region log-law constant (c.f. equation (4.17)) given by

$$C_o = \frac{1}{\kappa}\left\{\gamma_o - \log\left(\frac{\kappa}{a}\right) + E_1\left(\frac{aK}{\kappa^2}\right)\right\} - \sqrt{\frac{\pi}{2Ka}}\, e^{-aK/2\kappa^2}\, \mathrm{erfc}\left\{\sqrt{\frac{aK}{2\kappa^2}}\right\}. \tag{6.7}$$

In equations (6.6) and (6.7) erfc and E_1 denote the complementary error function and exponential integral, respectively and $\gamma_o = 0.577215\ldots$ is Euler's constant. The solution for the total enthalpy function Θ_1 is also given by equation (6.6) but with K and κ replaced by K_h and κ_θ respectively; in addition B_o, the outer region log-law constant for total enthalpy (c.f. equation (4.18)), replaces C_o. The constant B_o is also given by equation (6.7) but with $K = K_h$ and $\kappa = \kappa_\theta$.

7. Comparison with Experimental Data

In this section, the method of constructing composite profiles for total enthalpy and velocity will be described. Assume that at a given streamwise location along the surface, the following data are known: (a) the mainstream velocity U_e^*, temperature T_e^* and density ρ_e^*, (b) the wall temperature T_w^*, and (c) the incompressible displacement thickness δ^{**}. Note that a value for δ^{**} may easily be obtained from quoted experimental measurements of u/U_e in the boundary layer through numerical integration; it is related to the dimensionless thickness defined in equation (5.8) and used in the definitions (5.9), (5.14) and (6.2) by $\delta^{**} = L_{ref}^*\delta^*$. The specification of δ^{**} at a given streamwise location in effect defines a local length scale.

A Reynolds number based on the incompressible displacement thickness may now be defined by

$$Re_{\delta^*} = \frac{\rho_e^* U_e^* \delta^{**}}{\mu_w^*} = Re\,\frac{\rho_e U_e \delta^*}{\mu_w}, \tag{7.1}$$

and the match condition (4.19), using equation (6.2), becomes

$$\frac{1}{u_*} = \frac{1}{\kappa}\log\left\{Re_{\delta^*}\right\} + C_i - C_o. \tag{7.2}$$

Furthermore, the definition of displacement thickness equation (5.8) gives

$$\int_0^\infty \left(\frac{\rho_e}{\rho}\right)\left(1 - \frac{u}{U_e}\right)d\eta = u_* \ , \tag{7.3}$$

where the integral in equation (7.3) is across the entire boundary layer. It is easily shown, by integration of equation (6.4), that the constant a in equations is given by

$$a = - \frac{1}{F_{1\infty}}, \tag{7.4}$$

where $F_{1\infty}$ is the limiting value of $F_1(\eta)$ as $\eta \to \infty$. The value of a must be selected so that condition (7.3) is satisfied. It follows from equations (2.25) and (2.26) that

$$\frac{\rho_e}{\rho} = \left\{1 + \frac{(\gamma-1)}{2}M_e^2\right\}\left\{1 - \tfrac{1}{2}\,\alpha\, F^2\right\}, \tag{7.5}$$

where I and F are defined by equations (4.2). Therefore, the solution of equations (6.4) and (6.5) is coupled and an iterative solution for a is required in order to ensure that equation (7.3) is satisfied.

In practice, the iteration was carried out as follows. An initial guess was made for a and then $\partial F_1/\partial\eta$ and C_o were evaluated from equations (6.6) and (6.7). The inner variable Y^+ is related to η by

$$Y^+ = Re_{\delta^*}\eta, \tag{7.6}$$

and with u_* determined from equation (7.2), a composite profile for the velocity across the boundary layer is given by

$$F_{comp} = 1 + u_*\chi, \tag{7.7}$$

where

$$\chi = \frac{dF_1}{d\eta} + U^+(Y^+) - \tfrac{1}{\kappa}(\log Y^+ + C_i). \tag{7.8}$$

Now for the same value of a, an estimate of κ_θ was made and Θ_1 and B_o were obtained from equations (6.6) and (6.7). With B_i and C_i computed from the complete formulae in Appendix C with $T_B^+ = 110.2$ (or alternatively from the estimates (5.23) and (5.24)), κ_θ was evaluated from equation (4.23). Since B_o and B_i are functions of κ_θ, an iteration was carried out to determine a converged value of κ_θ which was then used to find the heat-transfer parameter q_* from equation (4.22). A composite profile for total enthalpy was then constructed according to

$$I_{comp} = 1 + q_*\left\{\Theta_1(\eta) + \theta^+ - \frac{1}{\kappa_\theta}\log\left(Y^+\sqrt{Pr}\right) - B_i\right\}. \tag{7.9}$$

Condition (7.3) becomes

$$\int_0^\infty \left.\frac{\rho}{\rho_e}\right|_{comp}\chi\, d\eta = -1, \tag{7.10}$$

where the first term in the integral was evaluated from equation (7.5) using the composite expansions (7.7) and (7.9) while the second term is given by equation (7.8). A trapezoidal rule on a nonuniform grid that expanded with distance from the wall was used to carry out the numerical integration; typically, 150 to 300 mesh points were found to give good accuracy. For a given value of a, the condition (7.10) will not, in general, be satisfied, and the value of a was then refined using an iterative procedure based on the secant method.

Direct comparisons were carried out with several sets of experimental data, and the theoretical profiles will be compared with nine representative profiles listed in Table 1. The first six profiles were taken from the data compiled in Reference 30 and here the same identification scheme is used; the first four digits identify an experiment while the last four designate a specific profile. Generally, profiles nearest the end of the test section were selected, since these were expected to be closest to self-similar conditions. In all cases, the velocity distribution was measured across the boundary layer, but tabulated temperature data were generally inferred from some version of the Crocco integral[30]. In Table 1, T_r represents the recovery temperature and $T_w/T_r = 1$ denotes an adiabatic wall. The present theory does not account for the influence of viscous dissipation; when $q_w = 0$, $H = H_e$ to leading order across the entire boundary layer (c.f. equations (3.19) and (4.8)). However, $H_w < H_e$ in all adiabatic-wall experiments and the difference $(H_e - H_w)$ increases with increasing M_e. In order to represent these cases here, the value of the wall temperature quoted in the experimental data[30] was used; this results in an analytical profile for total enthalpy with a very small value of q_* (c.f. Table 2). The case with $T_w/T_r < 1$ is a cold wall, while a value greater than 1 corresponds to a hot wall. The last three cases are taken from the recent data of Reference 17 where total temperature was measured directly.

Case No.	M_e	Re_{δ^*}	T_w/T_r
53011302	4.545	4241	1
53010401	2.54	2635	1
53010601	2.58	11607	1
74021805	4.50	17190	1
72040601	6.50	8436	0.5
73050504	10.31	42214	1.63
f-1048	2.16	6451	1.0
f-1548	2.17	5140	1.5
f-2048	2.14	4832	2.0

Table 1. Parameters associated with the experimental data.

Case No.	u_* (Experimental)	u_* (Theoretical)	q_* (Theoretical)
53011302	0.0544	0.0496	0.0048
53010401	0.0510	0.0478	0.0033
53010601	0.0426	0.0402	0.0027
74021805	0.0447	0.0415	0.0048
72040601	0.0464	0.0464	0.0300
73050504	0.0627	0.0453	- 0.0252
f-1048	0.0431	0.0421	0.0020
f-1548	0.0451	0.0445	- 0.0209
f-2048	0.0481	0.0459	- 0.0468

Table 2. Computed skin friction and heat transfer.

The comparisons with data for velocity are shown in Figure 1 where it may be noted that the agreement with the data is quite reasonable. It is worthwhile to note that closer correspondence with the data on a given profile can be achieved by adjusting the parameters in the turbulence models in equations (5.8) and (5.13), such as K and K_h. However, the objective here is to demonstrate that there is a degree of universality over a range of Mach numbers using the present models, and so no attempt to "fit" the data was made; the profiles were produced solely from the known physical quantities at each data station, as well as δ^{**}, and do represent the data reasonably well. At the same time, since true self-similarity will rarely be achieved in an experiment, a very close correspondence between the data and the theoretical profiles should not be expected. The total enthalpy profiles are given in Figure 2 where good comparisons may again be seen, even for the heated wall (case 7305) and the cooled wall (case 7204). Finally, the distributions of static temperature are shown in Figure 3 where again good agreement may be observed.

The calculated values of the skin friction parameter u_* are given in Table 2 and may be compared with the quoted experimental values. The experimental values of skin friction have been obtained by a variety of methods[30] (some of which are indirect) and generally involve errors of unknown magnitude. The theoretical estimates are reasonably close to the experimental values (except for the hypersonic case), with better correspondence occurring with the most recent measuurements. The heat transfer parameter q_* is also listed in Table 2 which, as anticipated, is very small and at least an order of magnitude smaller than u_* for the adiabatic cases; for flows with heat transfer, u_* and q_* are of comparable magnitude.

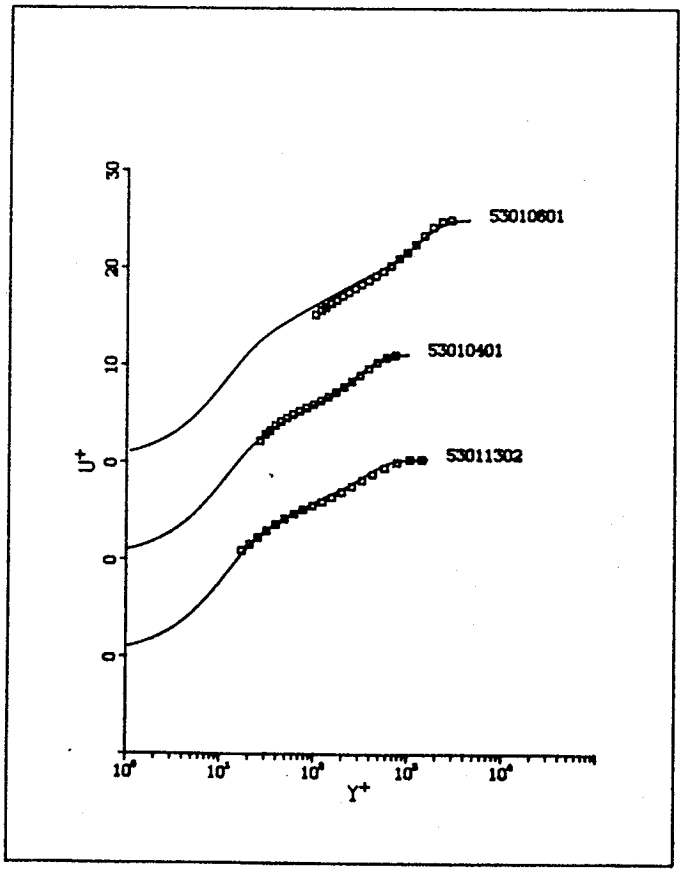

Figure 1. Comparison of velocity profile data with the theoretical profile. (Note the shifted origins). (a) Data from Reference 30.

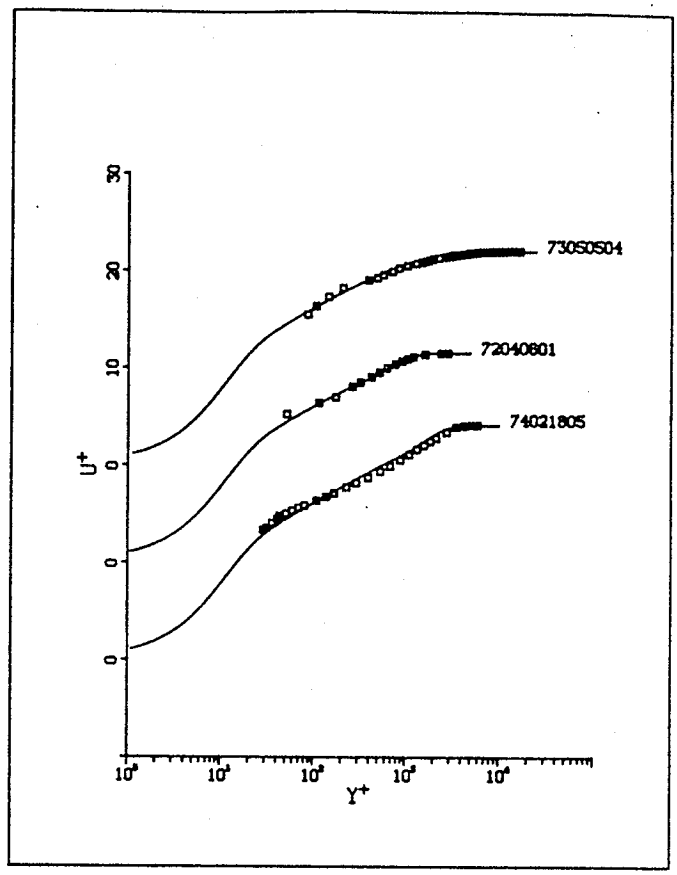

Figure 1. Continued. (b) Data from Reference 30.

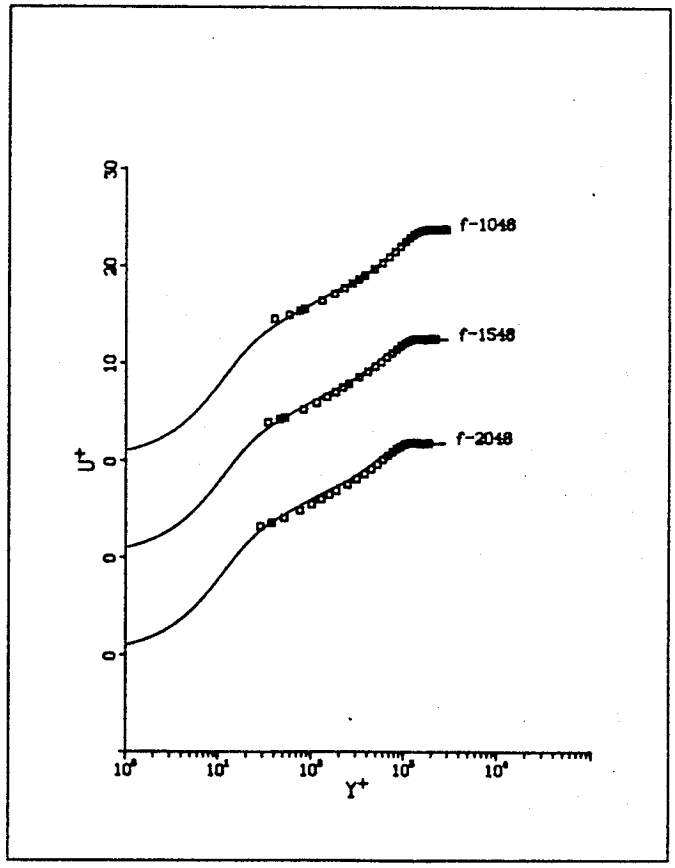

Figure 1. Continued. (c) Data from Reference 17.

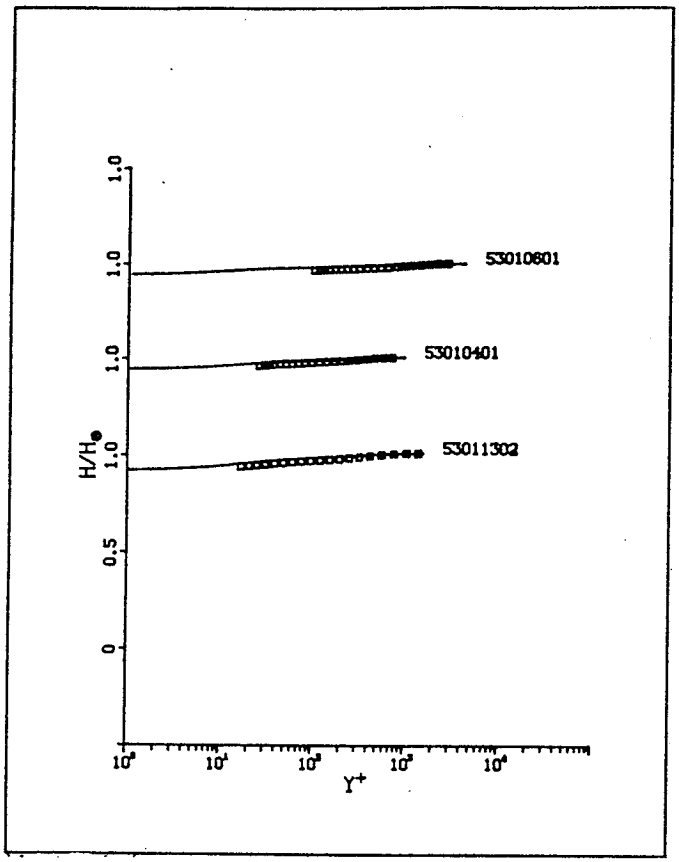

Figure 2. Comparisons with the total enthalpy profile. (Note the shifted origins.) (a) Data from Reference 30.

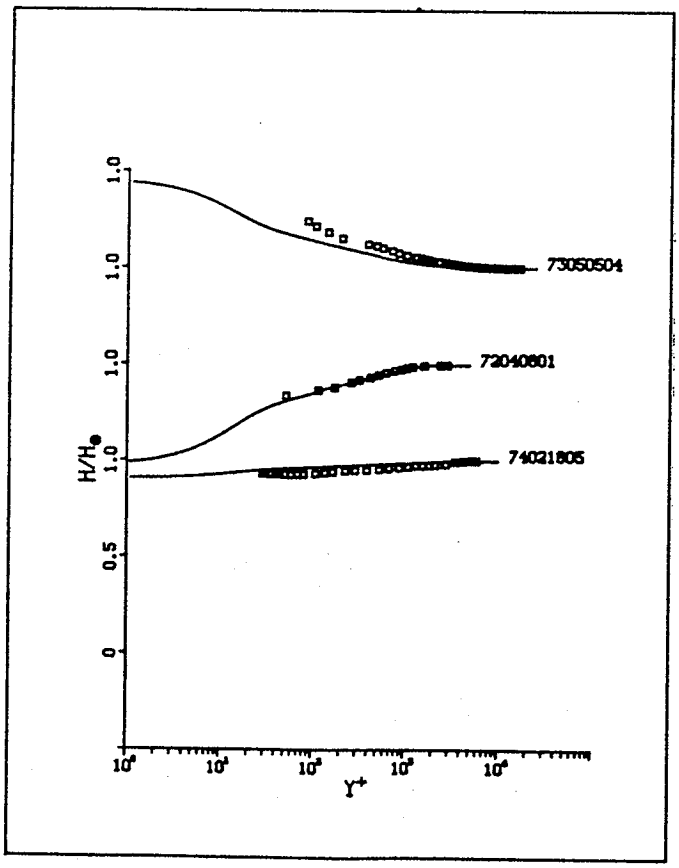

Figure 2. Continued. (b) Data from Reference 30.

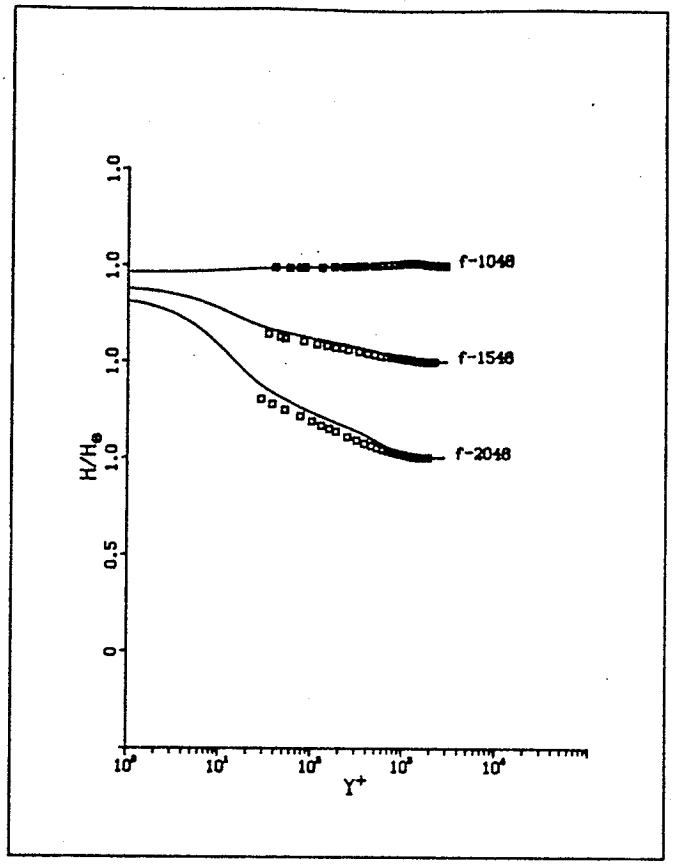

Figure 2. Continued. (c) Data from Reference 17.

8. Conclusions

In the present study, the new compressible turbulence models have been validated, and the embedded-function approach has been shown to be viable in the supersonic flow regime. In addition, a model for heat transfer in a high-speed compressible flow has been developed. One further byproduct of the present study is a set of composite velocity and total enthalpy profiles which gives a good representation across the entire boundary layer. These profiles could be used to define an initial distribution of the flow quantities to initiate a Navier-Stokes solution in a more general flow environment, simply by estimating displacement thickness distributions along all walls.

References

1. Cebeci, T. and Smith, A. M. O., Analysis of Turbulent Boundary Layers, Academic Press, New York, 1974.

2. Baldwin, B. S. and Lomax, H., "Thin-Layer Approximation and Algebraic Model for Turbulent Separated Flows", AIAA Paper 78-257, January 1978.

3. Mellor, G. L. and Gibson, D. M., "Equilibrium Turbulent Boundary Layers", *J. Fluid Mech.*, Vol. 24, p. 225, 1966.

4. White, F. M., Viscous Fluid Flow, McGraw-Hill Book Company, New York, 1974.

5. Kumar, A., "Numerical Simulation of Scramjet Inlet Flow Fields", NASA TP 2517, May 1986.

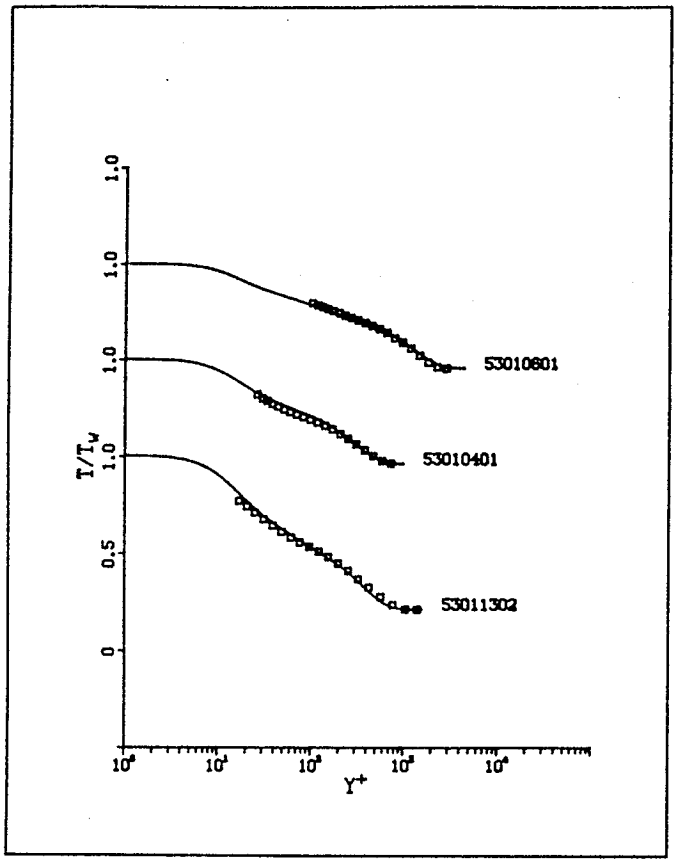

Figure 3. Comparison with the static temperature profile. (Note the shifted origins.) (a) Data from Reference 30.

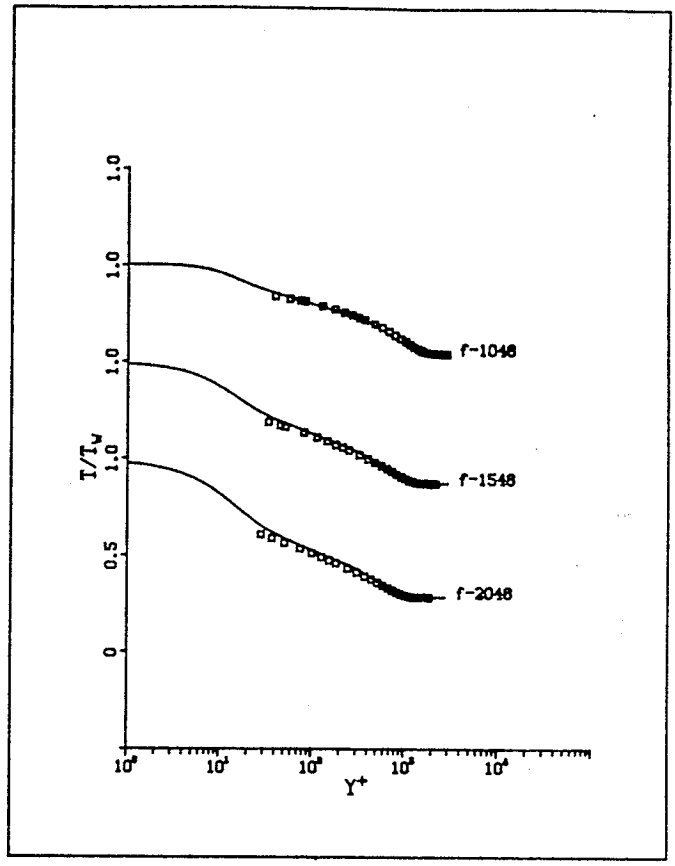

Figure 3. Continued. (c) Data from Reference 17.

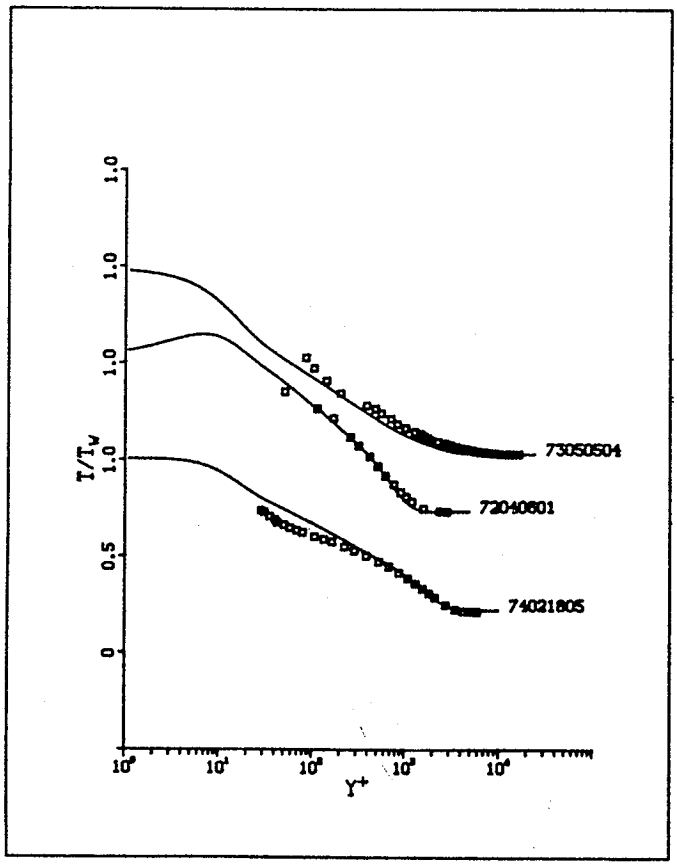

Figure 3. Continued. (b) Data from Reference 30.

6. Talcott, N. A. and Kumar, A., "Two-Dimensional Viscous Simulation of Inlet/Diffuser Flows with Terminal Shocks", *J. Propulsion*, Vol. 1, No. 2, pp. 103-108, 1985.

7. York, B. and Knight, D., "Calculation of a Class of Two-Dimensional Turbulent Boundary Layer Flows Using the Baldwin-Lomax Model", AIAA Paper 85-0126, Jan. 1985.

8. Viegas, J. R., Rubesin, M. W. and Horstman, C. C., "On the Use of Wall Functions as Boundary Conditions for Two-Dimensional Separated Compressible Flows", AIAA Paper 85-0180, Jan. 1985.

9. Carvin, C., Debieve, J. F. and Smits, A. J., "The Near-Wall Temperature Profile of Turbulent Boundary Layers", AIAA Paper 88-0136, Jan. 1988.

10. Rotta, J. C., "Turbulent Boundary Layers with Heat Transfer in Compressible Flow", AGARD Report 281, pp. 253-284, 1960.

11. White, F. M. and Christoph, G. H., *J. Basic Engrg.*, Vol. 94, pp. 636-642, 1972.

12. Van Driest, E. R., "Turbulent Boundary Layer in Compressible Fluids", *J. Aeronautical Sciences*, Vol. 18, pp. 145-161, 1951.

13. Maise, G. and McDonald, H., "Mixing Length and Kinematic Eddy Viscosity in a Compressible Boundary Layer", *AIAA J.*, Vol. 6, p. 73, 1968.

14. Weigand, G. G., "Forced Convection in a Two-Dimensional Nominally Steady Turbulent Boundary Layer", Ph.D. thesis, Purdue University, 1978.

15. Walker, J. D. A., Scharnhorst, R. K., and Weigand, G. G., "Wall Layer Models for the Calculation of Velocity and Heat Transfer in Turbulent Boundary Layers", AIAA Paper 86-0213, Jan. 1986.

16. Fernholz, H. H. and Finley, P. J., "A Critical Commentary on Mean Flow Data for Two-Dimensional Compressible Turbulent Boundary Layers", AGARD-AG-253, May 1980.

17. Carvin, C., "Etude Experimentale D'Une Couche Limite Turbulente Supersonique Fortement Chauffee", Ph.D. thesis, Universite' d'Aix Marseille, 1988.

18. Goldberg, U. and Reshotko, E., "Scaling and Modeling of the Three-Dimensional Turbulent Boundary Layer", *AIAA J.*, Vol. 22, p. 914, 1984.

19. Degani, A. T. and Walker, J. D. A., "Asymptotic Structure and Similarity Solutions for Three-Dimensional Turbulent Boundary Layers", AIAA Paper 89-1863, June 1989.

20. Wahls, R. A., Barnwell, R. W., and DeJarnette, F. R., "A Defect Stream Function, Law of the Wall/Wake Method for Compressible Turbulent Boundary Layers", AIAA Paper 89-00131, Jan. 1989.

21. Barnwell, R. and Wahls, R. A., "A Skin Friction Law for Compressible Turbulent Flow", AIAA Paper 89-1864, June 1989.

22. Walker, J. D. A., Werle, M. J. and Ece, M. C., "An Embedded Function Approach for Turbulent Flow Prediction", AIAA Paper 87-1464, June 1987; to appear in *AIAA J.*

23. Walker, J. D. A., Abbott, D. E., Scharnhorst, R. K. and Weigand, G. G., "Wall Layer Model for the Velocity Profile in Turbulent Flows", *AIAA J.*, Vol. 27, pp. 140-149, 1989.

24. Simpson, R. L., "A Model for the Backflow Mean Velocity Profile", *AIAA J.*, Vol. 21, pp. 142-143, 1982.

25. Walker, J. D. A., Werle, M. J., and Ece, M. C., "An Embedded Function Approach for the Calculation of Turbulent Flows Near Walls", UTRC 86-78, United Technologies Research Center, March, 1987.

26. Stewartson, K., The Theory at Laminar Boundary Layers in Compressible Fluids, Oxford University Press, 1964.

27. Fendell, F. E., "Singular Perturbation and Turbulent Shear Flow Near Walls", *J. Astro. Sciences*, Vol. 20, p. 129, 1972.

28. Mellor, G. L., "The Large Reynolds Number Asymptotic Theory of Turbulent Boundary Layers", *Int. J. Engng. Science*, Vol. 10, p. 851, 1972.

29. Melnik, R. G., "Turbulent Interactions on Airfoils at Transonic Speeds - Recent Developments", Computation of Viscous-Inviscid Interactions, AGARD-CP-291, Chapter 10, 1981.

30. Fernholz, H. H. and Finley, P. J., "A Critical Compilation of Compressible Turbulent Boundary Layer Data", AGARD-AG-223, June, 1977.

31. Walker, J. D. A. and Scharnhorst, R. K. "The Ξ Function", Department of Mechanical Engineering and Mechanics, Lehigh University, Bethlehem, Pennsylvania, Report FM-9, 1986; Air Force Office of Scientific Research, AFOSR-TR-1715TR (available NTIS-AD-A188680).

Appendix A

In this appendix, it is demonstrated that use of the Chapman-Rubesin law $\rho\mu = \rho_w\mu_w$ is consistent with the Sutherland relation (equation (2.13)) in the turbulent wall layer. At any streamwise location in the boundary layer, p is independent of n to leading order, and it follows that

$$\frac{\rho\mu}{\rho_w\mu_w} = \frac{T_w\mu}{T\mu_w} = \left(\frac{T}{T_w}\right)^{1/2}\frac{(T_w + S)}{(T + S)}, \tag{A.1}$$

for any fixed streamwise location s. But T/T_w is given by equation (2.27) in general, and using equations (3.9), (3.19), (4.12) and (4.22), it follows that

$$\frac{\rho\mu}{\rho_w\mu_w} = 1 + O(u_*). \tag{A.2}$$

Appendix B

In this appendix, the physical significance of each of the terms in equation (3.15) will be described. Let $\mathcal{L}^*$ denote a total energy loss, occurring within a control volume of unit length in the streamwise and spanwise directions and between the wall and a height n^*. Define $\mathcal{L}^*$ by

$$\mathcal{L}^* = \int_0^{n^*} \tau^*\frac{\partial u^*}{\partial n^*}dn^*. \tag{B.1}$$

However, if n^* is a location within the wall layer, τ^* is constant and thus $\mathcal{L}^* = u^*\tau^*$. A dimensionless total energy loss is defined by $\mathcal{L} = \mathcal{L}^*/(\rho^*_{ref}U^*_{ref}C^*_pT^*_{ref})$, and using equation (2.7) , it follows that within the wall layer

$$\mathcal{L}(Y^+) = (\gamma\text{-}1)M^2_{ref}\left\{\frac{\mu\rho}{\mu_w}u_\tau u\frac{\partial u}{\partial Y^+} + u\sigma\right\}. \tag{B.2}$$

The quantity $\mathcal{L}$ is positive and consists of two parts; the first term in equation (B.2) is associated with viscous dissipation into heat energy and corresponds to the second term in equation (3.15). The second term in equation (B.2) is associated with the production of turbulent kinetic energy. Define a dimensionless total flux due to molecular conduction (with respect to $\rho^*_{ref}U^*_{ref}C^*_pL^*_{ref}$) at height Y^+, *toward the wall*, by

$$q_{cond} = \frac{1}{Pr}\frac{\mu\rho}{\mu_w}\frac{\partial T}{\partial Y^+}, \tag{B.3}$$

which in view of equation (2.2) is equivalent to the last two terms on the right side of equation (3.15). Finally, define a total turbulent heat flux, *toward the wall*, by

$$q_{turb} = \rho\overline{v'T'}. \tag{B.4}$$

But in the present dimensionless variables

$$\rho\overline{v'T'} = \phi - (\gamma\text{-}1)M_{ref}^2 u\sigma, \tag{B.5}$$

and it follows that equation (3.15) is an energy balance which reads

$$q_w = q_{turb} + \mathcal{L} + q_{cond}. \tag{B.6}$$

Thus, the total energy conducted to the wall is balanced by the sum of the fluxes into the control volume at height Y^+ and the total energy loss within. For a hot wall $q_w < 0$ and for a cold wall $q_w > 0$.

Appendix C

In this appendix, the embedded functions for the wall-layer profiles of velocity and total enthalpy are summarized[15,23]; these profiles are analytical functions and a set of FORTRAN subroutines for their evaluation is available from the authors upon request. Both wall-layer profile models are of the form

$$U^+, \theta^+ = \left(1 + \frac{t_0^+}{T_B^+}\right)\left\{R(T_B^+,t_0^+)\, Q\,(\tilde{Y}^+) + Z(\tilde{Y}^+)\right\}$$

$$- \frac{t_0^+}{T_B^+}\left\{R(0,t_0^+)\, Q\,(\tilde{Y}^+) + Z(\tilde{Y}^+)\right\}. \tag{C.1}$$

Here t_0^+ is a parameter (to be determined) and T_B^+ is the mean period between bursts in the wall layer having a typical value[23] of $T_B^+ = 110.2$. The functions in equation (C.1) are given by:

$$R(t,t_0^+) = A_0 + \frac{a_0}{4}\log\,(t + t_0^+), \tag{C.2}$$

$$Q(Y) = (2y^2 + 1)\,\mathrm{erf}\, y + \frac{2}{\sqrt{\pi}}\, y e^{-y^2}, \tag{C.3}$$

$$Z(y) = \frac{2a_0}{\sqrt{\pi}}\left\{(2y^2 + 1)\,\Xi\,(y) + y\,\Xi\,'(y)\right.$$

$$\left. - \frac{\sqrt{\pi}}{8}(6y^2 + 1)\mathrm{erf}\, y \;-\; \frac{3}{4} y e^{-y^2}\right\}. \tag{C.4}$$

Here a_0 and A_0 are constants whose values are given by

$$a_0 = \frac{2}{\kappa}, \qquad A_0 = C_i - \frac{1}{\kappa}\left\{\frac{\gamma_0}{2} - \log 2\right\}, \tag{C.5}$$

for the velocity profile U^+, where C_i is the inner region log-law constant (c.f. equation 3.11), κ is the von Karman constant and γ_0 is Euler's constant. For the total enthalpy profile θ^+, replace κ with κ_θ and C_i with B_i in equation (C.5). For the velocity profile U^+, the normal variables appearing in equation (C.1) are

$$\tilde{Y}^+ = \frac{Y^+}{2\sqrt{T_B^+ + t_0^+}}, \qquad \tilde{Y}_0^+ = \frac{Y^+}{2\sqrt{t_0^+}}, \tag{C.6}$$

while for the enthalpy profile θ^+, Y^+ is replaced with Y_θ^+ in equation (C.6) (c.f. equation (3.23)). Finally, the function Ξ is defined by

$$\Xi(y) = \int_0^y e^{-z^2} \int_0^z e^{\xi^2} \int_0^\xi e^{-x^2}\, d\xi dx dz. \tag{C.7}$$

A list of the properties of this function is given in Reference 31 and, in particular, it may be shown that

$$\Xi(y) \sim \frac{\sqrt{\pi}}{4}\left\{\log y + \frac{\gamma_0}{2} - \frac{1}{4y^2} + \ldots\right\}, \quad \text{as } y \to \infty. \tag{C.8}$$

At the wall, the profile U^+ and θ^+ satisfy the first of equations (3.10) and (3.25); in addition, both profiles must satisfy the wall compatibility conditions[23] which are that the second and third profile derivatives must vanish at $Y^+ = 0$. For the velocity profile U^+, these conditions require [23] that

$$\sqrt{T_B^+ + t_0^+}\left\{R(T_B^+, t_0^+) - \frac{1}{\kappa}\right\} - \sqrt{t_0^+}\left\{R(0,t_0^+) - \frac{1}{\kappa}\right\}$$

$$= \frac{\sqrt{\pi}}{2}\, T_B^+, \tag{C.9}$$

$$(T_B^+ + t_0^+)^{-1/2}\, R(T_B^+, t_0^+) - (t_0^+)^{-1/2}\, R(0,t_0^+) = 0. \tag{C.10}$$

For the total enthalpy profile, κ_θ replaces κ in equations (C.9), (C.10) and (C.5) and B_i replaces C_i in equation (C.5); in addition, the right side of equation (C.9) is multiplied by $\sqrt{Pr}$.